

Simulation of Rosette Scanning Infrared Seeker and Counter-Countermeasure Using K-Means Algorithm

Sung-Gabb JAHNG[†], Hyun-Ki HONG[†], *Nonmembers*, and Jong-Soo CHOI^{††}, *Member*

SUMMARY The rosette-scanning infrared seeker (RSIS) is a tracker that a single infrared detector scans the total field of view (TFOV) in a rosette pattern, and then produces 2D image about a target. Since the detected image has various shapes in accordance with the target position in the TFOV, it is difficult to determine a precise target position from the obtained image. In order to track this type of target, therefore, we propose an efficient tracking method using the K-means algorithm (KMA). The KMA, which classifies image clusters and calculates their centers, is used to cope with a countermeasure (CM) such as an IR flare. To evaluate the performance of the RSIS using the KMA dynamically, we simulate the RSIS in the various conditions, and discuss the tracking results.

key words: *Rosette scan, seeker, counter-countermeasure, countermeasure, K-means algorithm*

1. Introduction

The rosette-scanning infrared seeker (RSIS), mounted on the thermal tracking missile, is a tracker that a single infrared detector scans the total field of view (TFOV) in a rosette pattern. The rosette pattern can be achieved by means of the two counter-rotating optical elements. Since the size of the instantaneous field of view (IFOV) is much smaller than that of the TFOV, the RSIS is less sensitive to the background noises than the reticle seekers [1]–[9]. If the RSIS has no infrared counter-countermeasure (IRCCM) against the countermeasure (CM) of the target such as a flare, however, it fails to track the target.

S.G. Jahng et al [10], [11] simulated the target tracking of the RSIS by using the moment technique. This method is to take an average of the target positions for a scan frame time. However, because this method can not distinguish the target from the flare, a presence of the flare makes it impossible to achieve a precise target tracking. W. Haifeng et al [12] proposed the tracking method using the projection technique to eliminate the effects of the CM. Although the RSIS detects the same target in size, it produces clusters of the various shapes according to the target positions in the

TFOV. Moreover, the scan velocity of the rosette pattern is not constant, which is fast at the center of the petal and slow at the tip. This scan velocity makes the interval between sample points unequal. For these reasons, the peak of the projected image may appear at the different position from the center of the target. In this case, therefore, the RSIS fails to track the target.

In this paper, we propose a new tracking method using the K-means algorithm (KMA) [13], [14]. Whenever the IR detector of the RSIS passes over the target and the flare, it produces the pulses, which are elements of the clustered image sets in the spatial coordinate. By using the KMA, elements of the detected image sets can be classified into two clusters: the target and the flare, and then a center of each cluster can be computed. Therefore, if the RSIS tracks only the target cluster center, then it eliminates the effects of the CM easily. When the target ejects two flares at the same time, however, the RSIS using the KMA fails to track the target because the KMA deals with the fixed number of clusters. In order to distinguish the target from two or more flares, we will present a tracking method using the ISODATA algorithm in the future work. To evaluate the tracking performance of the RSIS using the KMA, we simulate the RSIS in the various situations.

2. General Properties of the RSIS

The rosette pattern of the RSIS can be achieved by means of the two counter-rotating optical elements such as prisms, tilted mirrors, or off-centered lenses [1]–[3]. Figure 1 shows the scheme of the typical RSIS using wedge prisms with apex angle ϕ_1 and ϕ_2 , respectively. A prism of apex angle ϕ deviates a ray through a deviation angle δ as shown in Fig. 2. The deviation angle can be determined by using Snell's law of refraction as follow:

$$\delta \cong (\eta - 1)\phi, \quad (1)$$

where η is a refractive index. The deviation angle is also the radius of the TFOV.

The rotating elements spin at frequencies f_1 and f_2 , the values of which determine the scan pattern parameters such as the number of petals and the petal width. The loci of the rosette pattern at any time t , in cartesian coordinate, can be represented by

Manuscript received October 1, 1998.

Manuscript revised January 8, 1999.

[†]The authors are currently working toward Ph.D. degree in the Department of Electronic Engineering at Chung-Ang University, 221 Heuksuk-Dong, Dongjak-ku, Seoul, 156-756 Korea.

^{††}The author is with the Department of Electronic Engineering at Chung-Ang University, 221 Heuksuk-Dong, Dongjak-ku, Seoul, 156-756 Korea.

$$x(t) = \frac{\delta}{2} \cdot (\cos 2\pi f_1 t + \cos 2\pi f_2 t), \tag{2}$$

$$y(t) = \frac{\delta}{2} \cdot (\sin 2\pi f_1 t - \sin 2\pi f_2 t).$$

If f_2/f_1 is a rational number, then the pattern is closed, and f_1 and f_2 have a greatest common divisor f , such that $N_1 = f_1/f$ and $N_2 = f_2/f$ are both positive integers. Moreover, N_1 and N_2 are the smallest integers satisfying

$$\frac{N_2}{N_1} = \frac{f_2}{f_1}. \tag{3}$$

The rosette period, T , is $1/f = N_1/f_1 = N_2/f_2$. The number of petals in the pattern is $N = N_1 + N_2$. The size of the IFOV should be minimized to lessen interfering background signals and detector noise, but be large enough to provide full scan coverage (FSC). In order to design a small IFOV that achieves FSC, we apply the method of Ref. [15]. The size of the IFOV is defined as a distance between two points that are selected among the intersections between any petal and its neighbors. Therefore, the size of the IFOV (ω) can be represented as

$$\omega = \delta \cos(\pi/\Delta N) \sqrt{2 - 2 \cos(2\pi/N)}, \tag{4}$$

where $\Delta N = N_1 - N_2$ and $\Delta N \geq 3$. Figure 3 shows examples of the closed rosette pattern.

3. The Proposed Tracking Algorithm

The target signal detected by the IR sensor is a pulse sequence. This signal goes to the threshold circuit for separating the target and the background. If the intensity of the input signal is larger than the threshold level, then the output from the threshold circuit is normalized to one; otherwise, zero. The position of the detected signal at any sample time is calculated by Eq. (2), then stored to memory. The contents of the memory are elements of the clusters to form the 2D binary images as shown in Fig. 4(a). Since these images appear in various shapes according to their positions in the TFOV, it is impossible to distinguish the target from the flare. Figure 4(b) shows the projected image using the projection technique proposed

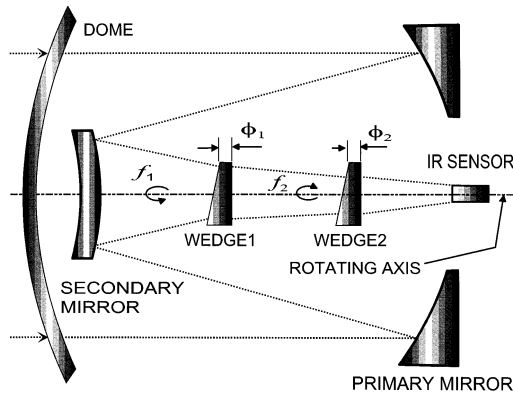


Fig. 1 Scheme of the RSIS.

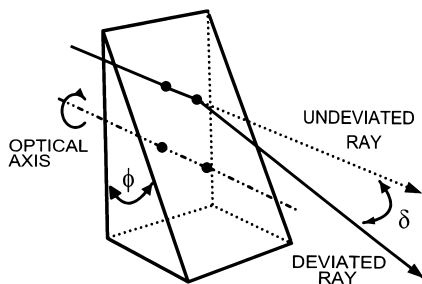


Fig. 2 Scheme of the wedge prism.

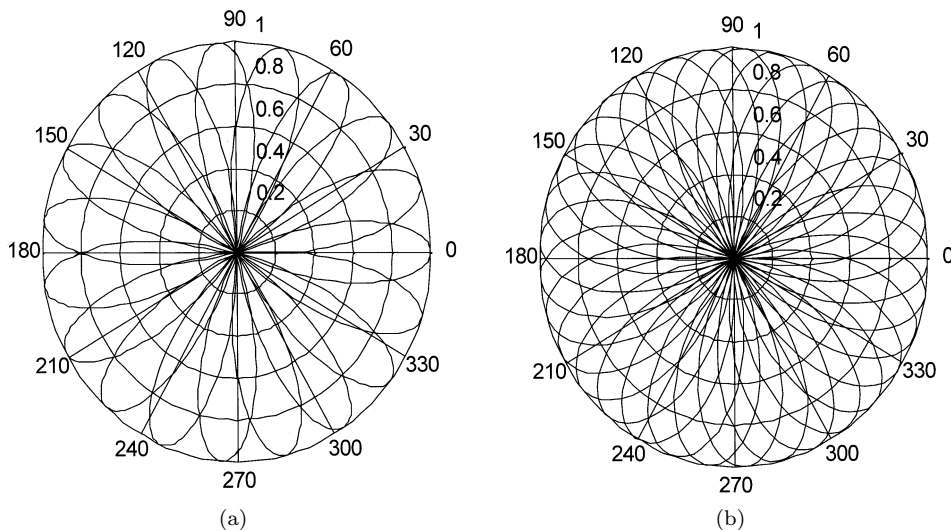


Fig. 3 Rosette patterns: (a) $N_1 = 12, N_2 = 7, \Delta N = 5$ (b) $N_1 = 23, N_2 = 10, \Delta N = 13$.

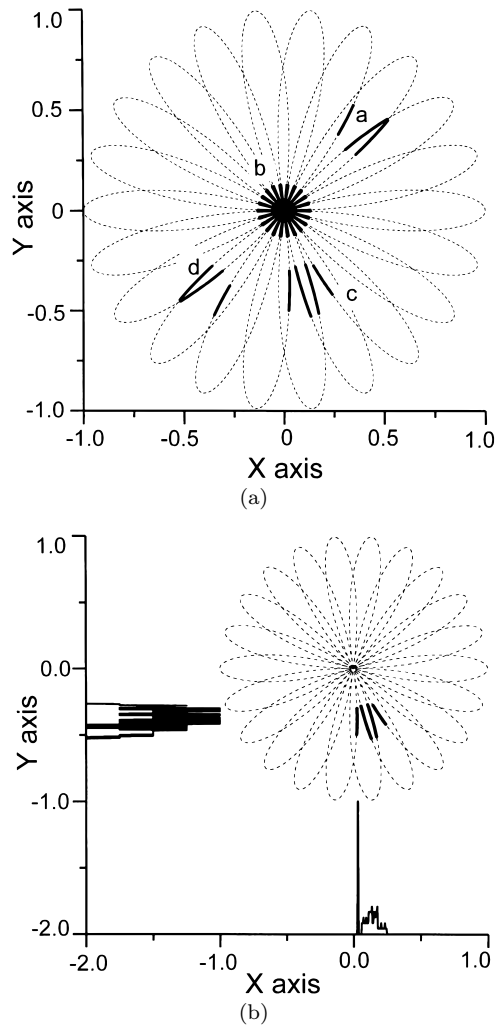


Fig. 4 (a) The detected images according to the various positions of the circular inputs: the radii of the circular inputs are all 0.0136 and their center positions are $a=(0.4, 0.4)$, $b=(0, 0)$, $c=(0.11, -0.4)$, and $d=(-0.4, -0.4)$, respectively. (b) The projected image of a cluster with respect to each axis.

by W. Haifeng et al. The center position of the original input image is $(x, y) = (0.11, -0.4)$. The peak value of the projected image is maximized where the samples are vertically distributed with respect to each axis. Unlike the original input center, the projected image of Fig. 4 (b) has the peak value at the position of $(x, y) = (0.015, -0.375)$. Since the projection technique uses the peak value to track the target, therefore, the RSIS can fail to track the target. Since the KMA computes the mean position of samples in a cluster regardless of sample distributions, however, the calculated center of a cluster shown in Fig. 4 (b) becomes $(x, y) = (0.103, -0.394)$, which is similar to the original input one.

By using the KMA, we can classify elements of the images into clusters, and then compute each cluster center. Therefore, the RSIS can track only the target cluster center without the effects of the flare. The KMA

is based on the minimization of a performance index that is defined as the sum of the squared distances from all points in a cluster domain to the cluster center. This procedure consists of the following steps [13], [14].

Step 1 Select K initial cluster centers $C_j(1), \dots, C_k(1)$. The subscript K stands for the cluster number. The initial cluster centers are usually selected as the first K elements of the given image set.

Step 2 At the n th iterative step distribute the elements $\{x\}$ among the K cluster domains, using the following relation,

$$x \in S_j(n), \text{ if } \|x - C_j(n)\| < \|x - C_i(n)\|, \quad (5)$$

for all $i = 1, 2, \dots, K, i \neq j$, where $S_j(n)$ denotes the set of elements whose cluster center is $C_j(n)$.

Step 3 From the results of **Step 2**, compute the new cluster centers $C_j(n+1), j = 1, 2, \dots, K$, such that the sum of the squared distances from all points in $S_j(n)$ to the new cluster center is minimized. The $C_j(n+1)$ which minimizes a performance index is simply the mean of $S_j(n)$. Therefore, the new cluster center is given by

$$C_j(n+1) = \frac{1}{N_j} \sum_{x \in S_j(n)} x, \quad j = 1, 2, \dots, K, \quad (6)$$

where N_j is the number of elements in $S_j(n)$.

Step 4 If $C_j(n+1) = C_j(n)$ for $j = 1, 2, \dots, K$, then the algorithm has converged and the procedure is terminated. Otherwise go to **Step 2**.

In general, the generated clusterings depend upon the choice of the initial cluster centers and the number of the specified cluster centers. If the CM does not operate, then only the target exists in the TFOV. So, K is 1 and the initial cluster center is the first elements of the target image set. If the CM operates, then the intensity of the flare is two to five times larger than that of the target during a flare function time [1], [2]. Therefore, the RSIS can recognize when the flare is ignited. In this case, K is 2 and the initial cluster centers are the first elements of the flare and the target image sets, respectively. Since the intensity of all elements are reduced to that of the target if the flare disappears out of the TFOV, K is 1 and the initial cluster center is the first elements of the target image set.

4. The Simulation Results

To evaluate the tracking method using the KMA dynamically, we simulate the RSIS using Matlab-simulink with the following assumptions: 1) both the target and the flare have circular shapes, which their diameters are 0.1 and 0.02, respectively, 2) their irradiances are uniform in the IFOV, and 3) atmosphere does not scatter and attenuate their irradiant energies.

Figure 5 shows a block diagram of the simulation.

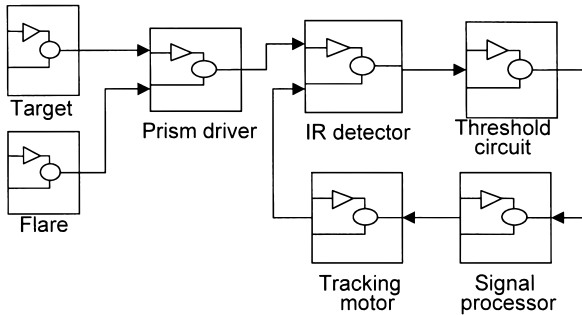


Fig. 5 Block diagram of the simulation.

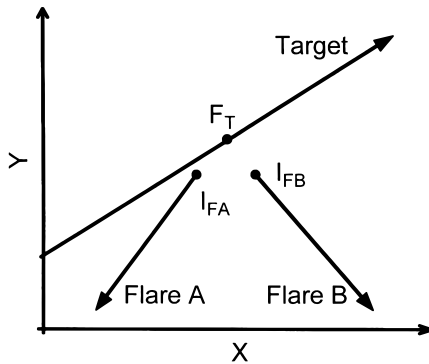
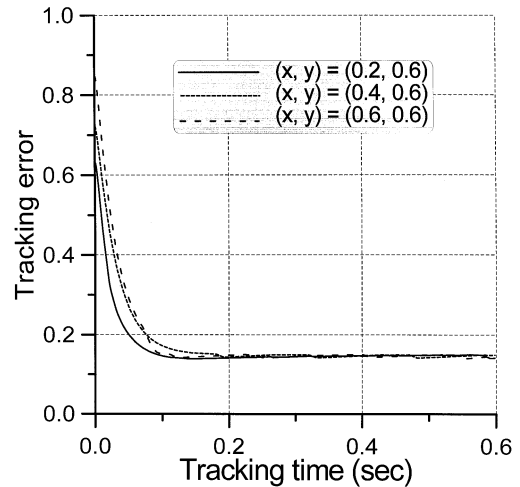


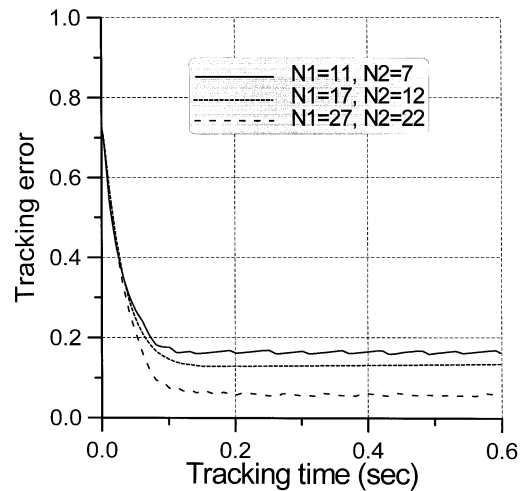
Fig. 6 Trajectories of the target and the flare.

The thermal signals radiated from the target and the flare are delivered to the IR sensor through two counter-rotating prisms. The output signal from the IR sensor is transferred to the threshold circuit eliminating the background noises. In the signal processor block, signals from the threshold circuit are classified into clusters, then each cluster center is computed by using the KMA. When the flare exists in the TFOV, the signal processor block can distinguish the target from the flare using the following data: the previous trajectory of the target and the sample numbers of the clusters. Since the motion of the target can not be abruptly changed, its next position is estimated using the previous trajectory and then the cluster nearest to the estimated position is selected as the target. Moreover, the target cluster has the larger samples than the flare cluster does since the size of the target is bigger than that of the flare. Using the obtained data, therefore, the signal processor block can discriminate the target from the flare easily. Only the cluster center recognized as a target is transferred to the tracking motor block, and then the RSIS can track the target without the effects of the CM.

The target and the flare move along the ramp trajectories as shown in Fig. 6. The target moves at a velocity of 1 scale a second (s/sec) in the x and y directions, respectively. Both the flare A and B are ejected in F_T at 0.3 s later after target tracking starts, and then fall at a velocity of 0.1 s/sec in the $-y$ direction. The



(a)

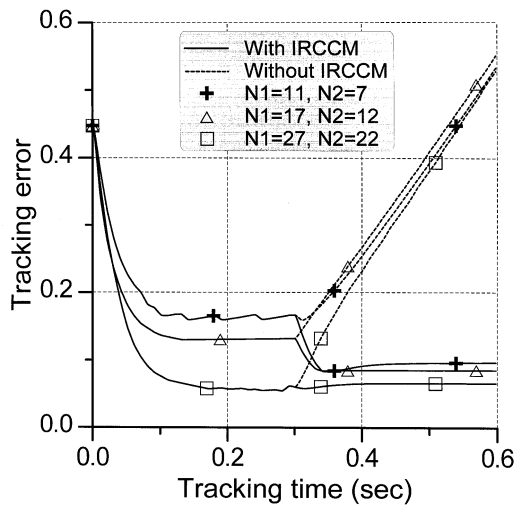


(b)

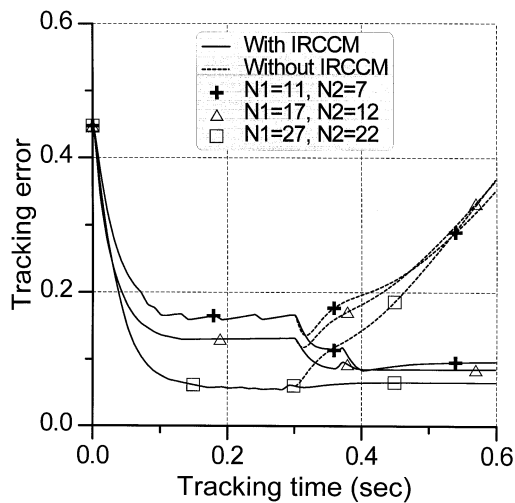
Fig. 7 Tracking performances without the CM operation: (a) for the various initial positions of the target; (b) for the various number of petals.

x axial velocities of the flare A and B are -0.1 s/sec and 0.1 s/sec, respectively. They are ignited at I_{FA} and I_{FB} , respectively, which are at 0.1 scale apart from F_T .

At first, we simulate the RSIS for the various initial positions of the target and for the various petal numbers of the rosette pattern without the CM operation as shown in Fig. 7. The tracking error shown in Fig. 7 is a squared distance between the center points of the target and the TFOV. Since the DC motor has a characteristic of a Type-1 system, its response for linearly moving input converges to a constant steady-state error. Figure 7(a) illustrates that the tracking errors for the various initial positions of the targets converge to a constant steady-state error. As the number of the petals increases, the RSIS has the good resolutions for images and the tracking performance. Therefore, as shown in Fig. 7(b), the tracking error of the RSIS with



(a)

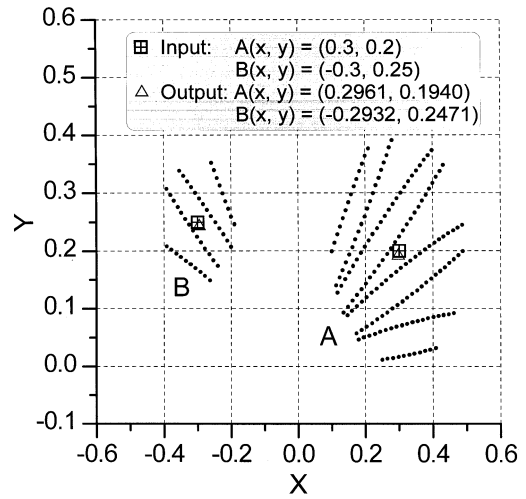


(b)

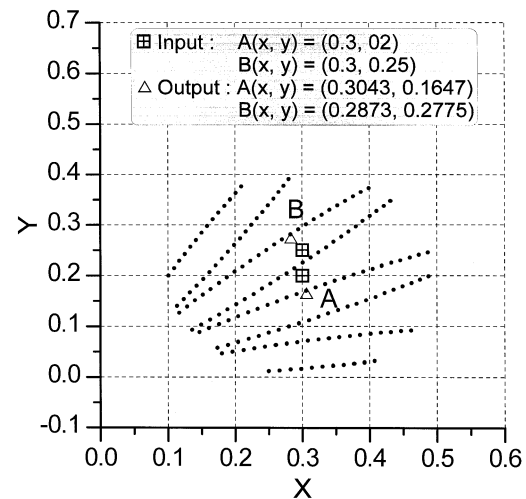
Fig. 8 Tracking performances of the RSIS with the CM operation: (a) the case of flare A; (b) the case of flare B.

$N = 49$ approaches closer to a zero steady-state error than that of any other. Figure 8 shows the tracking performances in the presence of the flare on the TFOV. The flares, ejected into the TFOV, move along the trajectories of the flare A and B as shown in Fig. 6, respectively. If the RSIS has no efficient IRCCM against the CM, then its tracking error increases and it fails to track the target as the dotted lines of Fig. 8. The solid lines illustrate the tracking errors of the RSIS using the KMA as the IRCCM. In this case, the tracking errors converge to constant steady-state errors by eliminating the effects of the flare efficiently.

In both of the cases $N = 18$ and 29 (solid lines each marked by crosses and triangles shown in Fig. 8), their steady-state errors converge close to zero after the flare is ejected. If two clusters are apart from each other as shown in Fig. 9 (a), then their calculated centers are



(a)



(b)

Fig. 9 The computed centers by the KMA for relative distances between two targets: (a) the targets at a long distance; (b) the targets within a short distance.

similar to those of the original inputs. On the other hand, if a distance between two clusters is too close to discriminate one from another, then the KMA results in estranging from each cluster center as shown in Fig. 9 (b). Therefore, the tracking error at the beginning of the flare ignition decreases, and then converges close to zero steady-state error. As the number of petals of the rosette pattern increases, the RSIS has the good resolutions for images in the TFOV. In this case, if two clusters do not coincide, then the KMA can classify them into the different clusters. Therefore, in the case of $N = 49$ (solid lines marked by rectangles shown in Fig. 8), the tracking errors result in converging to a constant steady-state error regardless of the presence of the flare.

When the target ejects two flares at the same time, the RSIS fails to track the target as shown in Fig. 10.

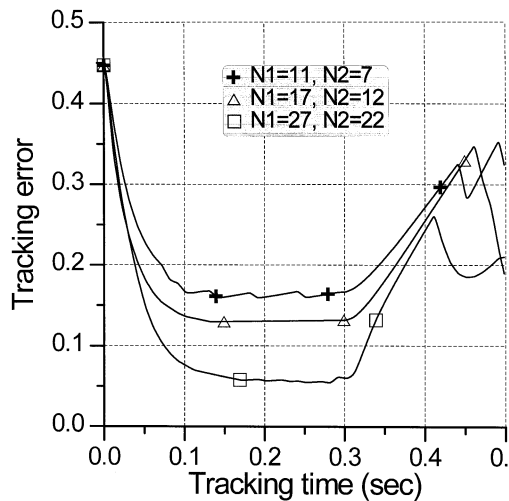


Fig. 10 Tracking performances of the RSIS in the presence of two flares.

Since the KMA deals with the fixed number of clusters, the K should be specified before the proposed IRCCM begins. In this paper, if the flare operates in the TFOV, then the K is set to 2; otherwise, K is set to 1. If two flares operate, then three clusters including the target exist in the TFOV. In this case, since the K is 2, the KMA recognizes two flare clusters as one flare, then miscalculates the cluster centers. Therefore, the RSIS fails to track the target. In order to eliminate the effects of two or more flares, we will study on a tracking method using the ISODATA algorithm [13], [14]. Unlike the KMA, the ISODATA algorithm does not deal with the fixed number of clusters but rather it deals with K clusters where K is allowed to range over the desired number of the clusters. It discards clusters with too few elements. Clusters are merged if the number of clusters grows too large or if clusters are too close together. A cluster is split if the number of clusters is too few or if the cluster contains very dissimilar elements. We expect that the ISODATA algorithm is a useful method to reduce the effects of the CMs with two or more flares.

5. Conclusion

In this paper, we have proposed a new IRCCM using the KMA to eliminate the effects of the IR flare. In order to examine the performance of the proposed tracking algorithm dynamically, we have simulated the RSIS using Matlab-simulink in the various cases. The simulation results showed that the RSIS achieved a precise target tracking regardless of the flare. However, we have known that the IRCCM using the KMA was susceptible to the number of the IR flares. In order to resolve this problem, future work will include a study on the ISODATA algorithm.

Acknowledgement

This work is supported by Automatic Control Research Center, Seoul National University, Seoul, Korea. The authors would like to thank Inn-Eark Yoo in Agency for Defense Development, Taejon, Korea, for helpful discussions.

References

- [1] J.S. Accetta and D.L. Shumaker, eds., "The infrared and electro-optical systems handbook," vol.7 and vol.3, SPIE Optical Engineering Press, Bellingham, Wash., 1993.
- [2] G.J. Zissis and W.L. Wolfe, eds., "The Infrared Handbook," ERIM Press, MI, 1993.
- [3] R.C. Hudson, "Infrared systems engineering," John Wiley & Sons, NY, 1969.
- [4] S.H. Han, H.K. Hong, and J.S. Choi, "Dynamic simulation of infrared reticle seekers and an efficient counter-countermeasure algorithm," *Opt. Eng.*, vol.36, no.8, pp.2341–2345, 1997.
- [5] H.K. Hong, S.H. Han, and J.S. Choi, "Simulation of the spinning concentric angular ring reticle seeker and an efficient counter-countermeasure," *Opt. Eng.*, vol.36, no.11, pp.3206–3211, 1997.
- [6] H.K. Hong, S.H. Han, and J.S. Choi, "Simulation of an improved reticle seeker using the segmented focal plane array," *Opt. Eng.*, vol.38, no.3, pp.883–888, 1997.
- [7] F.A. Rosell, "Prism scanner," *Journal of the Optical society of America*, vol.50, no.6, pp.521–526, June 1960.
- [8] T. Tajima, S. Wakabayashi, M. Kondo, and T. Takei, "Rosette scan infrared sensor," *Proc. SPIE*, vol.219, pp.51–57, 1980.
- [9] J.K. Bae, Y.H. Doh, D.S. Noh, and S.J. Kim, "Imaging system using frequency modulation/time division multiplexing hybrid reticle," *Opt. Eng.*, vol.37, no.7, pp.2119–2133, 1998.
- [10] S.G. Jahng, H.K. Hong, S.H. Han, and J.S. Choi, "Design of instantaneous field of view of the rosette scanning infrared seeker and dynamic simulation," *Proc. SPIE*, vol.3365, pp.158–168, April 1998.
- [11] S.G. Jahng, H.K. Hong, S.H. Han, and J.S. Choi, "Simulation of rosette scanning infrared seeker," *Proc. ITC-CSCC*, vol.2, pp.1765–1768, July 1998.
- [12] W. Haifeng, L. Zhi, Z. Qing, and S. Xinzhi, "A double band infrared image processing system using rosette scanning," *Proc. SPIE*, vol.2894, pp.2–10, 1996.
- [13] J.T. Tou and R.C. Gonzalez, "Pattern recognition principles," pp.75–109, Addison-Wesley Publishing Co., MA, 1974.
- [14] E. Gose, R. Johnsonbaugh, and S. Jost, "Pattern recognition and image analysis," pp.199–226, Prentice Hall, NJ, 1996.
- [15] S.G. Jahng, H.K. Hong, S.H. Han, and J.S. Choi, "Design and analysis of improved instantaneous field of view of rosette scanning infrared seeker," *Elect. Lett., IEE*, vol.33, no.23, pp.1964–1965, 1997.



Surng-Gabb Jahng was received BS and MS degrees in electronics engineering from Chung-Ang University, Seoul, Korea, in 1988 and 1990, respectively. He worked in Dong-in electronics co., Seoul, Korea, from 1988 to 1996. He joined the concurrent faculty at Bucheon College, Bucheon, Korea, in 1992. He is currently working toward Ph.D. degree in electronic engineering at Chung-Ang University. His

research interests are electro-optical systems, microprocessor appliances, and signal processing.



Hyun-Ki Hong was received the BS and the MS degrees from Chung-Ang University, Seoul, Korea, all in electronic engineering, in 1993 and 1995, respectively. He works on the Ph.D. degree in Department of Electronic Engineering, Chung-Ang University. His research interests are electro-optical systems, microprocessor appliances, and computer vision.



Jong-Soo Choi was received the BS degree from Inha University, Incheon, Korea, the MS degree from Seoul National University, Seoul, Korea, and the Ph.D. degree from Keio University, Yokohama, Japan, all in electrical engineering, in 1975, 1977, and 1981, respectively. He joined the faculty at Chung-Ang University in 1981, where he is now a Professor in the Department of Electronic Engineering. His current research interests are in

computer vision, image coding, and electro-optical systems.